Nano-Functionalized Electrochemical Sensors by Aerosol Jet Printing

Tiziano Fapanni, *Student Member, IEEE*, Emilio Sardini, *Member, IEEE*, Mauro Serpelloni, *Senior Member, IEEE*, and Sarah Tonello, *Member, IEEE*

Abstract*—Inthe latest years, hydrogenperoxidequantification gained a growing interest in many fields both in industry and in the clinical environment. Among the different available methods, electrochemical transducers are of particular interest thanks to their ease of fabrication, convenient integration with microfluidics and electronics and their time and cost-effectiveness. Despite these advantages, electrochemical transducers are affected by many metrological issues. In this work, the novel technique of Aerosol jet printing (AJP) is exploited to fabricate fully printed nanostructured electrochemical sensors for hydrogen peroxide detection. Two different carbon-based printable nanostructures, carbon nanotubes (CNTs) and graphene, are employed to conveniently modify with the same technique electrodes' surfaces. The performances of the proposed design, production process and the different functionalization are explored and discussed. After a preliminary evaluation of the electrochemical characteristicsof the printed devices, tests in hydrogenperoxideare carried on. Both materials present a limit of detections (LODs) and sensitivitycomparablewith the ones obtainedin the literature, even though CNT better performs than graphene in terms of sensitivity (20 versus 2.8 $\mu A\ mM^{-2}$). The latter presents however a signal-to-noise ratio (SNR) of 51.2 dB that outperforms the one of CNT (26.5 dB) and thus it has a better resistance against noise. Overall, both the evaluated nanostructures appear suitable to improve the metrological characteristics of printed electrochemical sensors and ease their spreading as environmental control devices, and diagnostic tools and assess quality in the industrial environment.

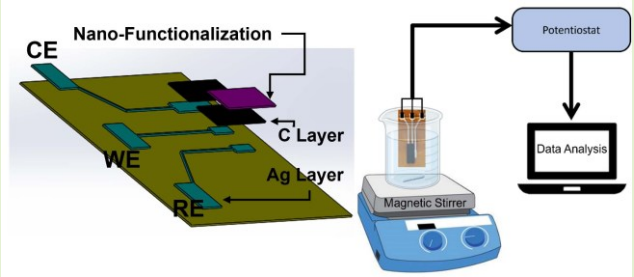

***Index Terms*—Aerosol jet printing (AJP), carbon nanotubes (CNTs), electrochemical sensors, graphene, hydrogen peroxide, nanostructures, printed sensors.**

I. Introduction

IN THE latest years, hydrogen peroxide reached a growing interest as an analyte in many fields as cellular processes, food control, clinical practice, and environmental control [1], [2], [3]. Moreover, hydrogen peroxide is a well-known byproduct in many biochemical reactions, usually mediated by an oxidase [4]. Hence, many different detection methods were developed to provide feedback on its concentration [5]. Among those, electrochemical transducers and electrochemical biosensors are of particular interest because they allow real-time and/or continuous monitoring of the concentration of an analyte in a solution, with quicker response times, easier methodologies, and fabrication than the standard detection methods. Moreover, they are easy to use, produce, and miniaturize. That improves their portability, eases on-site monitoring, and reduces the costs for the overall analytical process [6], [7], [8], [9], [10]. Despite these great advantages, electrochemical transducers are affected by many metrological issues, such as limited stability, selectivity, repeatability, and sensitivity [8], [10]. Most works in the literature aimed to address these issues by functionalizing the sensors with specific sensing layers, and thus, improving selectivity and sensitivity. These include biomolecules but also functionalization materials, such as ion-selective membranes, imprinted polymers, nanostructures, and microstructures [11], [12], [13]. Despite biomolecules offering unique advantages in terms of analyte recognition, they also introduce shelf life and storage issues that can limit their applicability outside of laboratory conditions [14]. A possible improvement that recently has gained great attention, in substitution or combination with bio-functionalization, is represented by surface micro- and nano-structuration of the electrodes, exploiting more stable nonbiological materials. Thus, by using those materials, properties can more easily be tuned depending on

Manuscript received 11 August 2022; revised 30 September 2022; accepted 30 September 2022. Date of publication 17 October 2022; date of current version 14 November 2022. The associate editor coordinating the review of this article and approving it for publication was Prof. Shaibal Mukherjee. *(Corresponding author: Tiziano Fapanni.)*

Tiziano Fapanni, Emilio Sardini, and Mauro Serpelloni are with the Department of Information Engineering, University of Brescia, 25123 Brescia, Italy (e-mail: t.fapanni@unibs.it; emilio.sardini@unibs.it; mauro.serpelloni@unibs.it).

Sarah Tonello is with the Department of Information Engineering, University of Padua, 35122 Padua, Italy (e-mail: sarah.tonello@unipd.it).

the specific application, with advantages in terms of durability. In particular, surface micro- and nano-structuration is explored and seems to be a promising methodology to improve the system sensitivity [10], [15] and amplify the sensors' signals [16]. Those techniques aim to increase the electrode-electrolyte interface and modify the mass transport processes in the proximity of the active electrodes [15], [17]. Different kinds of techniques as direct growth, photolithography, soft lithography, reactive ion etching, and recently 3-D printing, were explored to produce different micro-structured electrodes [18], [19], [20]. Nanomaterials are as well attracting great interest for their huge surface/volume ratio and their enzyme-mimetic effects [21], [22], [23]. Usually, the nanomaterials used for electrochemical biosensors are divided into two groups: carbon-based and noncarbon-based [17]. The latter presents a plethora of possible materials, including, for example, noble metals (such as silver, gold, and platinum), silica nanoparticles, and organic materials [24], [25], [26]. For their performances, commercial availability, as well as their low toxicity, carbon-based nanomaterials are, however, the most used in biosensing [27]. Thus, they represent an optimal trade-off among electrical properties, cost, and biological compatibility [28]. Of course, one of the most crucial aspects to fully exploit these properties to improve metrological issues of electrochemical biosensors is the possibility of precisely controlling the deposition of these functionalization materials. Thus, uncontrolled and often adopted deposition protocols lacking reproducibility and geometry control (e.g., manual drop-casting) might influence the variability of the final results. Among the techniques proposed in the literature for obtaining accurate and high-resolution patterns, the most relevant are electrochemical deposition and printing techniques. While the first requires an underneath layer already with the desired geometry, the second offers great versatility, both in terms of substrates and inks employed and of performance that can be achieved in terms of repeatability and resolution. Thanks to these characteristics, printed electronics is a promising technology for the production of sensors [29]. Among the wide variety of printing techniques, the most promising to realize accurate functionalization patterns on top of electrodes are mask-less techniques (e.g., inkjet (IP), aerosol jet printing (AJP), laser-induced forward transfer (LIFT), microprinting and nanopen printing). These technologies rely on ink dispensing through openings or nozzles and define structures by moving the stage in a preprogramed pattern [10]. Among the possible techniques, AJP was selected for this application both in continuity with previous work [1], [15] and thanks to its technical characteristics. In particular, using these fully additive, noncontact production techniques can improve the fabrication process for this novel kind of sensor, allowing its simplification and increasing process control. Moreover, thanks to AJP's unique process flow, material waste can be reduced to a minimum, and micrometer-scale resolutions can be achieved in digitally controlled complex patterns both on planar and 3-D surfaces [30], [31].

As reported in the literature, most of those advantages are granted by its peculiar noncontact production process that uses gases to atomize, carry, and focus the functional inks. The production process control is performed by adjusting three flows: atomizer (that generates the aerosol and acts as a carrier), exhaust (that controls the dimension of the particles), and sheath (that focuses the aerosol on the nozzle). The first two allow selecting how much ink is deposed, while the latter shapes the linewidth and helps in avoiding clogging events [32]. In this work, the production process of a simple, fully printed nanostructured electrochemical cell is proposed. AJP was used to fabricate the whole device starting from the bare cell deposition and then using two different carbon nanostructures to functionalize the WEs. The aim was to provide a more general investigation of sensors as possible, as a starting point for translating sensor use in any areas previously mentioned (e.g., cellular processes, food control, clinical practice, and environmental control). The printed sensors were tested, and the two different nanostructures were compared to evaluate their electrochemical behavior and how they can improve the characteristics of the sensors.

II. Materials and Methods

A. Design and Production Process

A three electrodes layout, including a working electrode (WE), reference electrode (RE), and counter electrode (CE), was selected as the most commonly used electrochemical sensor to guarantee optimal control of the potential of the cell. This kind of device relates the output current to the concentration of analytes that undergo redox reactions close to the active electrodes. Starting from previous work [1], [15], we designed simple cells with parallel rectangular electrodes. The sensor was fabricated by means of three different inks, deposed during three successive printing sessions. Silver-silver chloride ink (AgCl ink, XA-3773, Fujikura Kasei Company Ltd., Tokyo, Japan) was employed to fabricate conductive tracks, pads, and the RE, to ensure high conductivity, as well as RE stability; carbon ink (C ink, EXP 2652-28, Creative Materials Inc., Ayer, MA, USA) was selected for WE and CE to provide a stable electrochemical substrate, as well as a suitable substrate for further functionalization; finally, two different kinds of nanostructures were selected for the surface functionalization: carbon nanotubes (CNTs) or graphene. An explicative render design is shown in Fig. 1(a). The CNT functionalization was otherwise performed using the commercial Nink 1000 (Nanolab, Waltham, MA, USA) Multiwalled CNTs ink. This is an aqueous suspension of multiwalled CNTs with a declared length between 1 and 5 μm and a diameter of 15 nm. The graphene coating was obtained by exploiting a custom ink developed to ensure both printability and adhesion on the substrates. The ink was prepared by loading 15% of graphene powder and adding 3% of polyvinylpyrrolidone (PVP) as binder and adhesive. To improve the printability and lower the ink viscosity, 38.5% of deionized (DI) water and the same amount of ethyl glycol were added. Furthermore, to avoid the agglomeration of the solid particles, 5% dispersant was added. Different curing parameters were evaluated to provide an optimal curing process that requires a 20-min thermal treatment at 200 °C. This ensures a good ink-substrate adhesion even in wet environments. The graphene powder was acquired by Directa Plus S.p.A. (Lomazzo, Italy), which

TABLE I
AJP PROCESS PARAMETERS

	AgCl Ink	C ink	CNT ink	Graphene Ink
Sheat flow (SCCM)	250	910	50	80
Atomizer flow (SCCM)	1100	1300	670	630
Exhaust flow (SCCM)	1040	1000	580	550
Printing speed (mm/s)	2.5	2.5	2	2
Plate temperature (°C)	75	75	45	90
Curing time (min)	30	15	20	20
Curing temperature (°C)	125	175	60	200
# of depositions	1	6	3	9
Head size (μm)	750	750	300	300

produces it through a patented process. The obtained power has a mass-median-diameter (D_{50}) of (4 ± 2) μm. An Aerosol Jet Printer (AJ300, Optomec, Albuquerque, NM, USA) with a 750 μm head was employed to fabricate the bare devices. This technique was selected as the production process because it allows deposing of all the needed materials in a digitally controlled manner that ensures fast prototyping and production. A parallelized production protocol was implemented to reduce intersensor variability. In detail, for each lot, ten devices were printed in two rows within the same printing session. Thirty bare electrodes were produced and divided into three lots named A, B, and C. Flexible polyimide foil of 75 μm (Kapton, DuPont de Nemours, Luxembourg, Grand Duchy of Luxembourg) were selected as substrate, due to its excellent mechanical properties and good compatibility with inks and printing process. For each lot, the substrate was at first cleaned in ethanol to remove possible contaminants and increase the adhesion between ink and substrate. After that, AgCl ink was deposed and cured at 125 °C for 30 min. Next, WE and CE were coated with carbon ink and then cured at 175 °C for 15 min. Finally, WE was AJP-functionalized using a 300 μm head and CNT (sensors 1–5) and graphene (sensors 6–10) inks. Those carbon-based nanostructures were chosen to improve the sensitivity of the sensors. According to the literature, such nanostructures are able to increase the surface-to-volume ratio even without changing the chemical composition of the surface [10], [33], [34]. Moreover, the selected digital production process aims to improve the repeatability of the printed sensors avoiding operator-dependent drop-casting functionalization methods [35], [36]. Both the nanostructured inks were thermally cured for 20 min before testing. Lot A and B were used to perform preliminary adhesion and electrochemical tests, while lot C was used to evaluate sensor performance for peroxide detection. The final sensors fabricated are shown in Fig. 1(b), while the selected process parameters are reported in Table I.

B. Preliminary Process Evaluation

After the production process, different tests were carried out to evaluate its goodness. At first, different geometrical evaluations were performed using an optical microscope NB50T (Orma Scientific, Sesto San Giovanni, Milan, Italy) with a trinocular zoom of 0.8×–5× light-emitting diode (LED). Then the geometrical profiles of the active electrodes were evaluated using an Alpha-Step IQ Surface Profilometer (KLA-Tencor, Milpitas, CA, USA) in four different positions. At last, a set of scratch tests were carried out to ensure the correct adhesion of the printed materials on the substrate. Briefly, a set of lines were scratched on the surface of the sacrificial electrodes using a metal blade. Then, a Kapton tape is placed in contact with the devices and removed three times. A visual examination was then carried out to assess the adhesion between the substrate and the selected inks.

C. Preliminary Electrochemical Assays

After the first physical assays, different tests were carried out on analyzing the electrochemical behavior of the devices. All the following tests were performed using a portable potentiostat Palmsens3 EIS (Palmsens, Compact Electrochemical Interfaces, Houten, Utrecht, The Netherlands). At first, a set of cyclic voltammetry (CV) experiments were carried out in a phosphate-buffered saline (PBS) to evaluate the suitable potential windows of the sensors with a different functionalization. The test was performed by running different CVs with a fixed scan rate (υ = 0.2 V/s). From previous works [15], a starting [−0.05, 1] V potential window was selected, and then it was gradually increased until unwanted features, such as peaks unrelated to the electroactive analytes in the solution (spurious peaks), were recorded. The suitable potential window selected is the last one where no spurious peaks were recorded. Then a set of CVs was carried out in a ferro/ferricyanide ($[Fe(CN)_6]^{3-/4-}$) solution in PBS to evaluate the voltammograms and to further inquire about the microscopic surface area of the electrodes according to [1]. Briefly, different CVs were carried out in ferro/ferricyanide solutions at different concentrations (2, 4, 6, and 8 mM) at a fixed scan rate (υ = 0.2 V/s). The shape of the voltammograms was evaluated, and the peak position and amplitude were compared between the different surface functionalizations. To evaluate the surface area, the CVs on 8 mM ferro/ferricyanide in PBS solution were considered. From Randles-Sevcik equation (1), the electroactive surface area was calculated using the well-known electrochemical parameters of the ferrous/ferric redox couple, as its diffusion coefficient ($D = 6.20 \cdot 10^{-6}$ cm^2/s), number of active electrons (n = 1), as well as the physical constants (Faraday's constant F and the universal gas constant R) and the measured values for the peak current I_p and absolute temperature (T)

$$I_p = \pm 0.446 nFAC^*(nFD\upsilon/RT)^{0.5}. \quad (1)$$

Furthermore, the stability of the electrodes was assessed. One electrode for each functionalization was exposed to a ferro/ferricyanide solution (6 mM in PBS), and a set of four CVs (inside the previously defined potential windows, scan rate υ = 0.2 V/s) were performed every 2 min for nine times. The peak current was evaluated in time and compared with the ones obtained with a commercial Screen-Printed Carbon Electrode (DRP-C11L, Metrohm Dropsens, Asturias, Spain). Moreover, a set of electrodes were immersed in PBS, and single chronoamperometry (CA) (applied voltage 1 V) was performed. The experiment aimed to estimate the time needed to obtain a steady-state current. This time is unique for each electrochemical system since it is influenced by

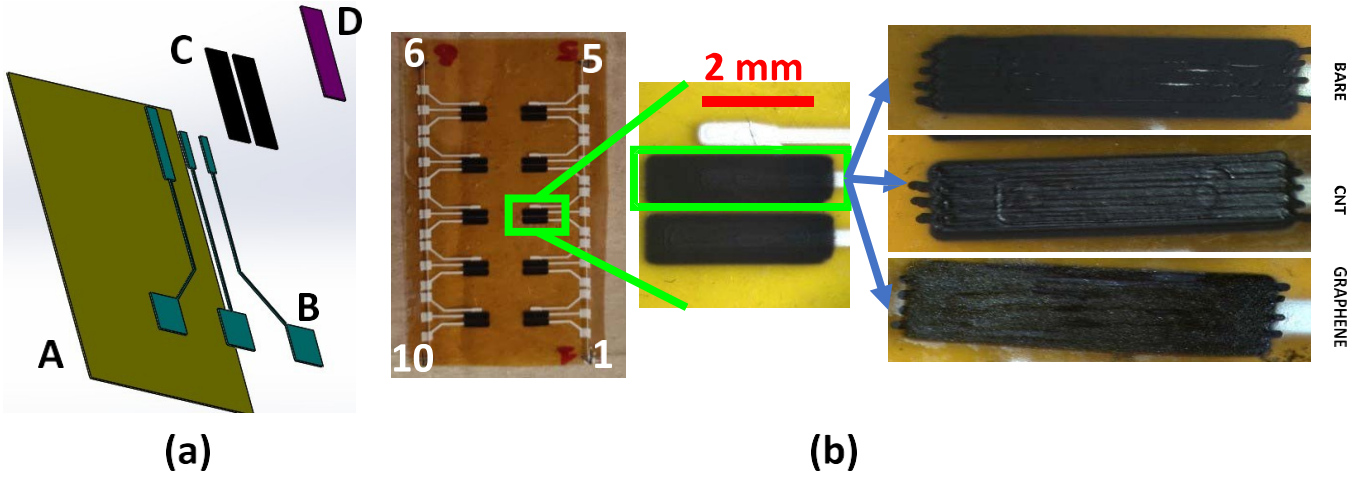

Fig. 1. (a) Render design (in fake color to enhance visibility) of the sensors (a) showing the layers composing the sensor. A: Substrate. B: Silver-silver chloride traces and RE. C: WE and CE carbon layers. D: WE nano-functionalization. In (b) the printed devices at different scales are reported.

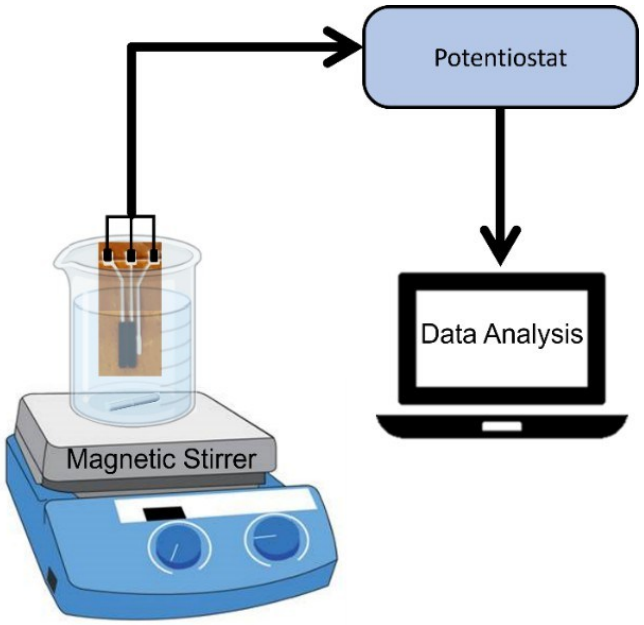

Fig. 2. Experimental setup used to detect hydrogen peroxide. The sensor (orange) is placed inside a backer filled with PBS. This setup is placed on top of the stirrer. The Palmsens3 reads the information on the device and sends them to a laptop, where the information is stored and later analyzed.

several different factors depending on the electrolyte solution (species and its hydrodynamics), the analytes (number of transferred electrons and the species diffusion coefficient), and the electrodes (shape, dimensions, materials, resistance, surface roughness, and porosity) [37]. Hence, this parameter has been estimated to plan further analysis accordingly.

D. Peroxide Detection

To perform these experiments, the electrodes were immersed in 20 mL of PBS stirred at 490 r/min through an ARGO LAB M2-D Pro magnetic stirrer (Giorgio Bormac S.r.l., Carpi, Italy). This experimental setup is exemplified in Fig. 2. The electrodes first underwent a pretreatment step that is composed of a 300 s long CA at 1 V followed by 20 CVs at 0.2 V/s scan rate and using the potential windows defined in the previous experiment (see preliminary electrochemical evaluations). Then, hydrogen peroxide detection was performed through CA. After waiting for 600 s to reach the steady-state current, hydrogen peroxide was injected in steps of 100 μM until the total amount of 500 μM was achieved. Each concentration step was maintained for 200 s. The applied potential was set above the oxidation peak obtained from the voltammogram analysis at 1 V for each kind of electrode. The collected signals were elaborated through a MATLAB 2019b. The current values were evaluated by averaging the last 20 s of each concentration step. From the collected data, the noise was extracted as already proposed in [38]. Briefly, noise is extracted by subtracting the average steady-state current of the sensors from the measured steady-state current. The former was considered the signal level of the sensors. Those two values were compared to evaluate the signal-to-noise ratio (SNR) of the electrodes. Moreover, the noise signal was evaluated in the frequency domain calculating its power spectral density (PSD).

III. Experimental Results

A. Preliminary Process Evaluation

The preliminary evaluations on the electrodes using the optical microscope provided interesting information on the output of the production process. The correct coating of the WE and CE electrodes was assessed, as well as the physical dimensions of the interconnecting lines that resulted (495 ± 30) μm wide, including a reduced phenomenon of overspray. A set of images collected with the optical microscope can be seen in Fig. 1(b), where the three different WEs used are shown. There, differences in color and texture are visible. In fact, the bare electrode resulted darker and opaque, the CNT-functionalized one is shinier, and the graphene-functionalized one presented a glitter-like appearance. Then, the mechanical profilometer was employed to assess the thickness of the produced electrodes in four different positions on all lot C sensors. The profiles

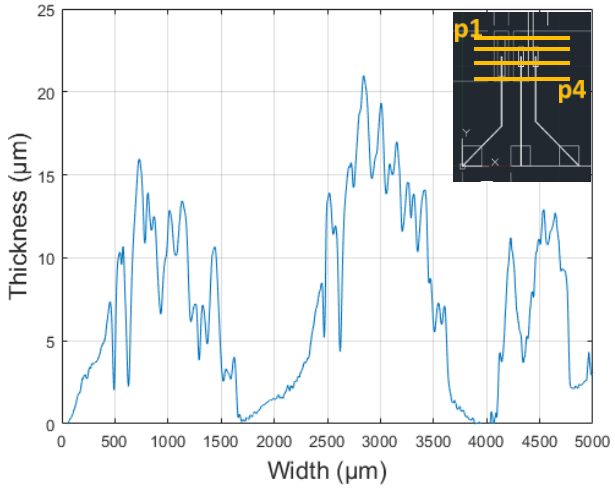

Fig. 3. Profile of the electrodes (from left to right CE, WE, and RE) achieved with the mechanical profilometer in position p2. The four position in which the profiles were sampled are depicted (inset).

TABLE II
SELECTED POTENTIAL WINDOWS

Functional Ink	E_min (V)	E-max (V)
Bare Carbon	-0.05	1.3
CNT	-0.05	1.0
Graphene	-0.15	1.0

obtained in position p2 can be seen in Fig. 3. The average profiles reflect the designed layer structure. The profiles taken in positions 2 and 3 that depict the center of the electrodes have similar shapes, and they present an average thickness of 7.43 μm for CE. 11.33 μm for WE and 6.36 μm for RE. No appreciable difference between CNT and graphene-functionalized electrodes is observed. The peaks measured on position p1 have different thicknesses due to their different design. CE is the thickest due to the overlay of the silver/silver chloride and the carbon layers, WE only presents the carbon layer, while the RE result is invisible since no layer is present. Last, the scratch test was carried out on the sacrificial electrodes. No appreciable difference was observed after the test, and thus, the results (shown in Fig. 4) confirm the adhesion between each layer of the device and between the printed layers and the substrate.

B. Preliminary Electrochemical Assays

Results obtained from the first experiment performed allowed us to obtain the potential window for each kind of electrode we produced. The voltammograms obtained are shown in Fig. 5. All the electrodes present a spurious peak at around 0.1 V that appears to increase the lower bound of the window. According to this observation, for each kind of electrode, a potential window was selected to avoid those unwanted features. The potential windows, summarized in Table II, are adopted for all the following experiments.

C. Cyclic Voltammetry

CV was carried out in ferro/ferricyanide solutions in various concentrations ranging from 2 to 8 mM. The obtained voltammograms are shown in Fig. 6. All the voltammograms

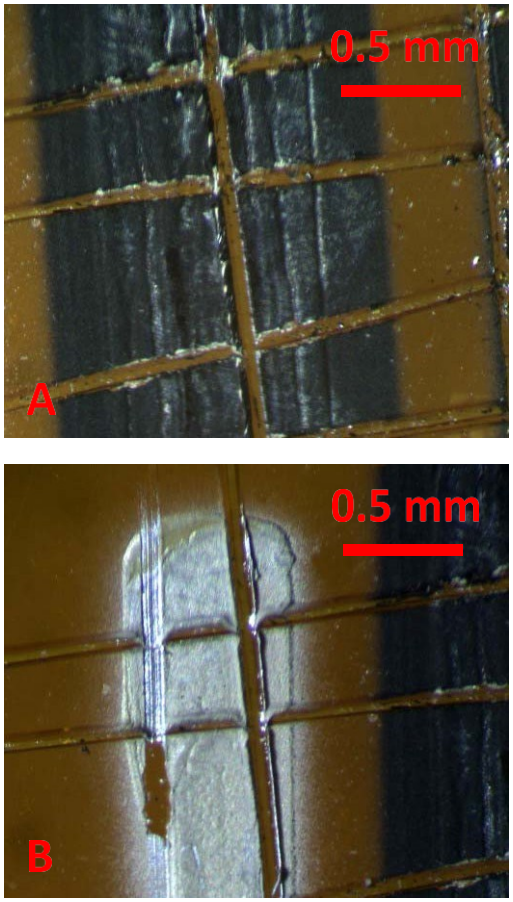

Fig. 4. Optical images obtained on the sacrificial electrodes after the scratch test for (a) CE and (b) RE.

present detectable oxidative peaks at well-defined potentials. CNT-functionalized electrodes show better performances presenting a fully reversible behavior, the lowest peak voltage at (180 ± 5) mV, and the highest sensibility. Graphene presents an oxidative peak of around (455 ± 20) mV. The stable potential windows for those electrodes do not allow a complete formation of the reduction peak. Similar observations can be made for the voltammograms produced by the bare carbon electrodes where the peak voltage is located around (974 ± 17) mV. The voltammograms were also used to obtain information about the active surface area of the electrodes. According to those calculations, graphene-functionalized electrodes were able to improve the microscopic surface area 11.27 times more than the original bare electrodes, while CNT improved the microscopic area up to 105.56 folds.

D. Stability Tests

Electrode stability was assessed by evaluating the peak current over time (see Fig. 7). All the examined electrodes present similar behavior, with an absolute value of the peak height increasing over time at each CV sweep. This trend is also present in commercial screen-printed electrodes (SPEs). This data underlines how stability, and consequently, reusability might be the future challenge to be addressed to improve the overall behavior of these devices [10], [39] as far as CV is selected as a measurement technique. Then, the stability

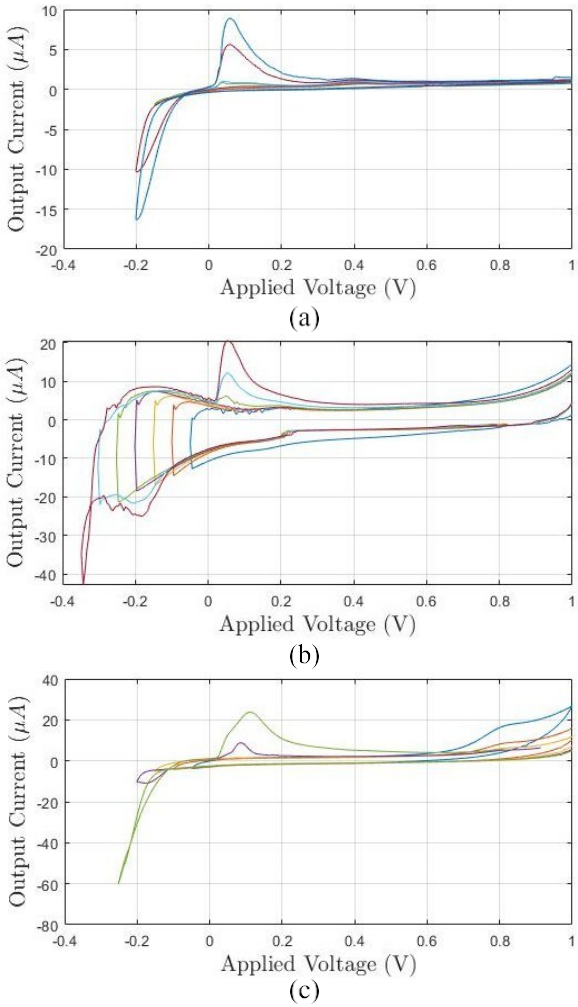

Fig. 5. Potential windows definition test for (a) bare carbon electrodes, (b) CNT, and (c) graphene functionalized.

and settling time in chronoamperometric measurements was evaluated. Both the nano-functionalized electrodes produced a similar steady-state current. We considered the current at its steady state when the signal derivative was lower than 0.01 μA/s. This situation occurs after approximately 400 s for each kind of sensor.

E. Peroxide Detection

CA experiments were carried out for all the produced sensors in lot C. An example of the obtained output current is shown in Fig. 8(a). All the calibration lines obtained from these experiments are reported in Fig. 8(b). All the produced sensors produced a linear calibration line ($R^2 > 0.9$). The average sensitivity of CNT functionalized sensors resulted in (20 $\pm$ 4) μA/mM with a relative standard deviation of 0.2, while graphene functionalized sensors produced an average sensitivity of (2.8 $\pm$ 0.9) μA/mM with a relative standard deviation of 0.33. Furthermore, the response time of the sensors was estimated by stepping up the pure PBS solution to a concentration of 100 μM. The response time was defined as the time needed for the output current signal to go from 10% to 90% of its steady state. The behavior of all the printed sensors was evaluated and averaged. The two kinds of functionalization behave similarly and produce a fast response of (3 $\pm$ 1.5) s for CNT electrodes and of (2.5 $\pm$ 1.7) s for graphene ones. It is important to notice that the main factor that impacts the response time variability is the position in which the solution is injected and is thus highly operator dependent. Although the variability of the measurements is up to 70%, the response time of the device is comparable with other works in the literature [2], [40]. Moreover, different levels of noise were

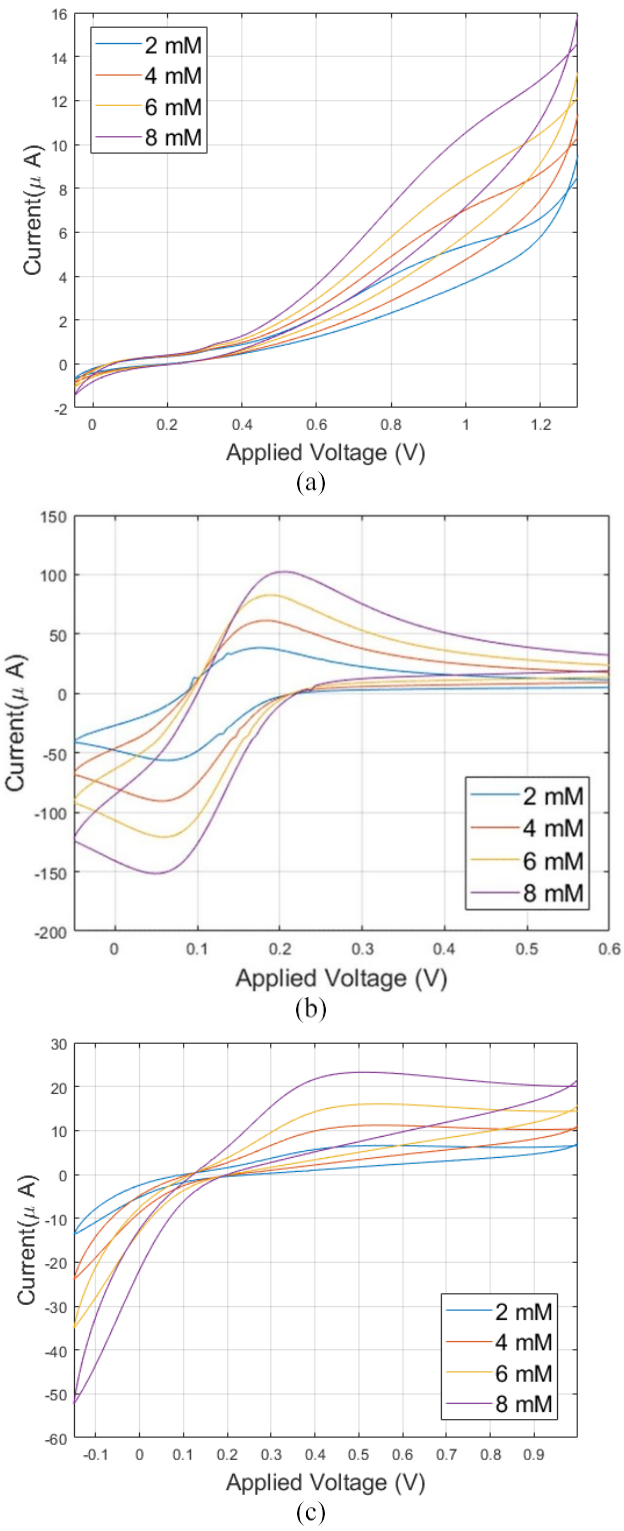

Fig. 6. Voltammograms obtained with ferro/ferricyanide for (a) carbon bare, (b) CNT, and (c) graphene electrodes.

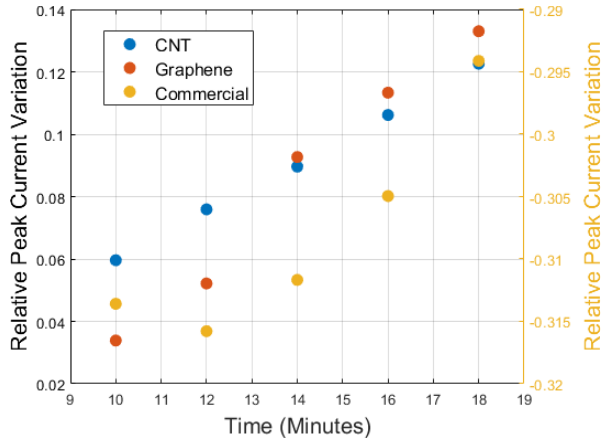

Fig. 7. Normalized peak current of CVs (υ =0.2 V/s) recorded every 2 min in 6 mM ferro/ferricyanide solution for CNT functionalized electrodes (blue), graphene functionalized electrodes (red), and commercial SPE (yellow, secondary y-axis).

recorded on the signal from the different sensors. On average, the SNR for the sensors functionalized with CNT was 26.5 dB, while the one for the ones functionalized with graphene was almost double at 51.2 dB. A more accurate analysis of the noise produced by CNT sensors obtained as described in Section II was carried out and an example of its PSD is shown in Fig. 9. All the sensors present a similar PSD with a constant spectrum at low frequency, with a flicker-like behavior above approximately 1 Hz. Different analyte concentrations slightly change the overall power of the noise, shifting up the plot on the y-axis.

IV. Discussion

Results obtained during sensors characterization offered the opportunity to discuss several interesting and promising aspects concerning both the electrochemical behavior of the specific materials employed (inks and nanomaterials) and the overall performances of the electrochemical sensors while quantifying hydrogen peroxide. According to the results obtained during the preliminary electrochemical characterization, the spurious peak around 0.1 V observed in all the sensors represents an interesting effect for being discussed. This effect is probably due to the electroactivity of the silver/silver chloride layer underlying WE and CE in the presence of the supporting electrolytic solution. In detail, due to the chemical properties of silver-silver chloride, when it is polarized at a negative potential in the presence of an ionic solution, it attracts electrons, thus causing oxidation of the material. This results in the measurement of an oxidative peak of current originating from the interaction between the supporting electrolyte and the conductive electrode. Since this peak is completely independent of the concentration of the analyte in the solution, it represents a typical sign of instability and has to be avoided in the stability window to make sure that all the peaks measured are only due to analyte presence. Similar effects are reported in the literature even when using silver/silver chlorides RE [41]. This issue might be reduced by modifying the production process and introducing a third layer composed of a different noble metal ink such as silver, gold, or platinum, which are stable in the potential window of interest. In the

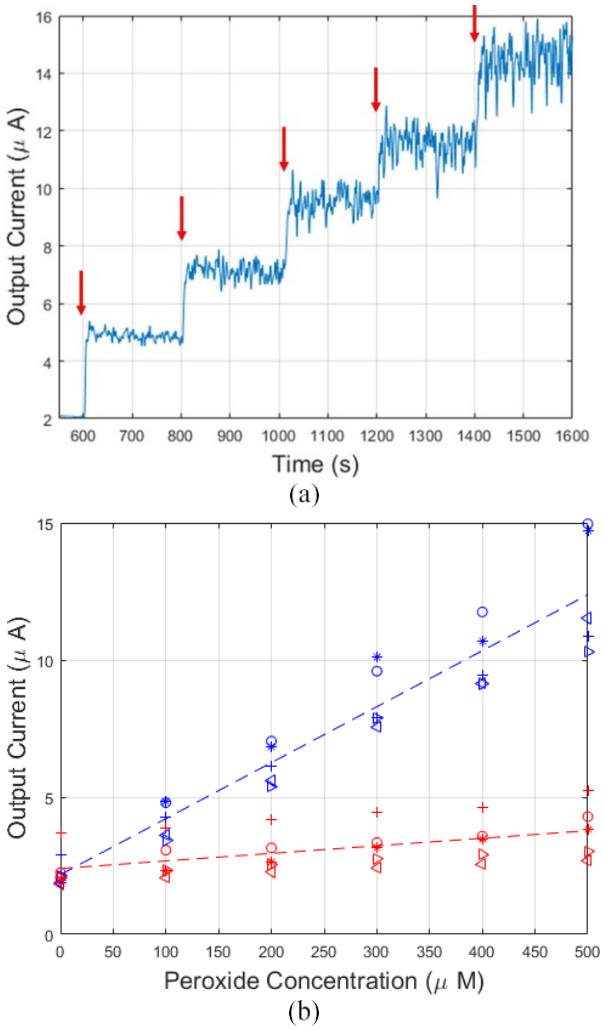

Fig. 8. (a) CA responses for a graphene-functionalized sensor with injections of 100 μM of hydrogen peroxide at the time instants marked by red arrows. The calibration curves extracted for each sensor are reported in (b) where dashed lines represent the average fitting line for each electrode functionalized with CNT (blue) and graphene (red).

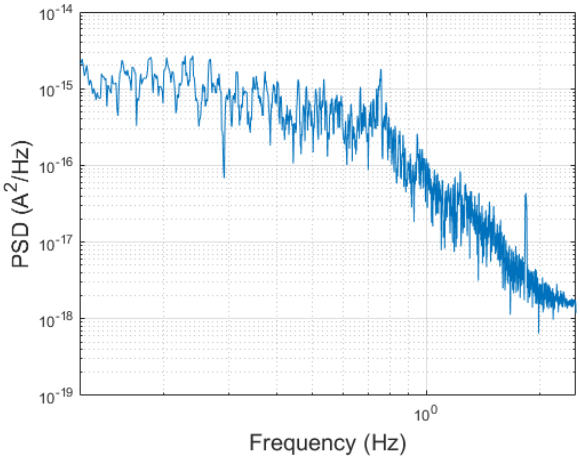

Fig. 9. PSD of the noise produced by a CNT-functionalized sensor on a single concentration interval.

current application, however, the potential of interest required to detect hydrogen peroxide (1 V) falls within the potential windows ([−0.05, 1] V) in which the combination between

solution and electrodes materials is stable, and the system does not show any significant spurious current peaks. The absence of any peaks other than the one of ferro/ferricyanide in this window confirms that our results are reliable and robust. Moreover, it ensures the possibility of relying on the selected fabrication process, which is faster and more cost-effective with respect to a traditional three-layer structure with stacked silver, carbon and silver chloride. Despite the presence of the spurious peak, thanks to the accurate definition of a stable window potential, the CVs in ferro/ferricyanide revealed stable peaks voltages that are related to the surface functionalization, as well as the RE material, the used electrolyte solution, ohmic drop and electrode resistance [41]. We report a decrease in the peak voltage for the CNT and graphene functionalization. Those effects are also reported in the literature and can be explained considering the different diffusion patterns involved and the change in the electrode-electrolyte interface resistance [25], [35], [42]. A major difference comparing presented results with the literature regards graphene-functionalized electrodes. For example, in [43], small to no difference between bare and functionalized sensors as regards the peak position, while the ones presented here are highly reduced. The difference can be explained by considering both the different production processes and the different materials employed. As an example, the cited work employs a glassy carbon electrode that is way more conductive than our printed ones, and then graphene is electrodeposited on top of the electrode. This process introduces small to no differences in the electrode resistance. On the other hand, the hereby proposed devices are composed of printed electrodes that present lower conductivity, and then the use of a nanostructured functionalization widely reduces the electrode/electrolyte resistance. This produces a remarkable decrement in the standard potential of the reaction [37]. As regards the current produced by the sensors during peroxide detection, different values were obtained according to their nano-functionalization. CNT helped increase the total output current up to 15 μA, producing also better sensitivity, while graphene produced a maximum current of 5 μA in similar conditions. As already observed in [15], there is a linear correlation between the increased sensitivity of the devices and their surface area. Moreover, nanoparticles increased the surface area of the electrodes much more than the previously reported microstructures. Although, those two approaches are valid and could be used together to further improve the sensitivity of electrochemical devices. The sensitivity of the sensor was improved by increasing the surface-to-volume ratio of the electrode-solution interface, thanks to the nanotubular geometry of CNTs, to the large sheets geometry of graphene layers randomly oriented during the deposition. Results obtained reveal that CNTs perform better than graphene in improving the sensitivity producing an average sensitivity of around (27 ± 5) μA/(mM cm^2) rather than (3.5 ± 1.3) μA/(mM cm^2) obtained with the latter. Those values are, on average, smaller than the ones obtained in the literature presented in Table III, but that can be due to the on-site synthesis of those devices versus our ink deposition and/or the use of different nanostructures that further enhance the sensitivity of the reported devices. Similar observations can be made with regard to the limit of detection (LOD) of the sensors. The intrasensor LOD of our devices was determined according to [44] and reported, as well as in Table III. The LOD of the two kinds of functionalization presents small differences and is comparable with the ones already reported in the literature. The variations can be again due to different processes and interface resistance that can impact the overall SNR of the devices.

TABLE III
COMPARISON OF THE VALUES OF THE LIMIT OF DETECTION (LOD) AND SENSITIVITY BETWEEN DIFFERENT WORKS IN LITERATURE AND OUR DEVICES

	LOD (μM)	Sensitivity (μA mM^{-1} cm^{-2})	Ref.
rGO-MWCNT	9.4	32.91	[48]
rGO	0.7	22.78	[40]
rGO	1.0	300.00	[46]
MWCNT-PT	0.3	205.80	[45]
CNT	7.3	27.00	This work
Graphene	8.8	3.50	This work

The main differences in sensitivity and LOD between the sensors presented in this work and the best ones presented in the literature [45], [46] is due to different production processes, growth of the functionalization materials, and different kinds of nanostructures involved. For instance, in [45], a set of nanohybrids composed of CNTs and platinum nanoparticles were synthesized through a time-consuming approach that involved strong acids. Those nanoparticles were then dropcasted on a bulk platinum electrode. Otherwise, in [46], direct growth of graphene nanostructures was achieved through an electrochemical process that required a highly controlled setup. Indeed, these techniques provide better metrological characteristics, but with the approach proposed in this work, it is possible to highly reduce the use of dangerous chemicals, and at the same time, to reduce the time duration of the process production. Moreover, with the hereby proposed approach, different patterns can be digitally designed and achieved, allowing fast prototyping of innovative devices with characteristics that are a tradeoff between metrological and processing ones.

As regards the noise recorded on the sensors, different features were observed. Analyzing the standard deviation of the signal at the different analyte concentrations, a linear correlation between the two parameters was recorded, which was more evident on CNT-functionalized sensors. Analyzing their PSD (see Fig. 7), we could observe the superposition of two different effects. At low frequencies, thermal and shot noise dominate. Both those effects produce a white noise with a power that is directly proportional to the average current flowing on the electrochemical cell, and this explains the increase of noise at higher concentrations. At higher frequencies, mass transport effects are relevant. Those processes are involved in providing analytes to the surface of the electrodes where the reaction occurs, and thus, can shape the PSD of the correlated noise [47].

V. Conclusion

In this work, a comprehensive comparison between the electrochemical performances of CNT and graphene-modified electrodes was reported. Significant differences were highlighted both in the preliminary characterization tests and in the detection of hydrogen peroxide. Although similar limits of detections were achieved (7.3 μM for CNT and 8.8 μM for graphene) and both were able to improve the electrode-electrolyte interface area up to 105 times, CNT produced on average, a better sensitivity (20 μA mM^{-2}) than graphene (2.8 μA mM^{-2}), while both the functionalization layer presented response times comparable with the literature, although presenting a high variability. The introduction of an automatized process or microfluidic system could be implemented in the future to try to reduce the underlined variability. According to the presented results, both the nanostructured inks taken into consideration appear suitable to improve the sensitivity, and in general, the metrological characteristics of printed electrochemical sensors. Overall, the proposed fabrication process, which includes all the fabrication steps starting from bare electrodes to their surface functionalization, appears particularly convenient, in terms of time and cost-effectiveness, to ease the integration of fully printed electrochemical sensors in devices for environmental control, diagnostic monitoring and to assess quality in the industrial environment. Further inquiries can be addressed to evaluate the effects of both microstructures and nanostructures on the metrological characteristics of electrochemical devices, as well as to deepen the understanding of the noise and uncertainty produced by electrochemical transducers.

References

[1] S. Tonello et al., "Preliminary study of a flexible printed multisensing platform for electromyography and lactate measuring during rehabilitation," in *Proc. IEEE Int. Symp. Med. Meas. Appl. (MeMeA)*, Jun. 2021, pp. 1–6, doi: 10.1109/MeMeA52024.2021.9478729.

[2] K. Promsuwan et al., "Micro-colloidal catalyst of palladium nanoparticles on polyaniline-coated carbon microspheres for a non-enzymatic hydrogen peroxide sensor," *Microchem. J.*, vol. 171, Dec. 2021, Art. no. 106785, doi: 10.1016/j.microc.2021.106785.

[3] M. Carbone, E. Aneggi, F. Figueredo, and S. Susmel, "NiO-nanoflowers decorating a plastic electrode for the non-enzymatic amperometric detection of H_2O_2 in milk: Old issue, new challenge," *Food Control*, vol. 132, Feb. 2022, Art. no. 108549, doi: 10.1016/j.foodcont.2021.108549.

[4] J. H. Chang, S. Y. Shen, C. Di Dong, M. Shkir, and M. Kumar, "Morphology-dependent MoO_3/Ni–F nanostructures with enhanced electrochemical hydrogen peroxide detection," *Chemosphere*, vol. 287, Jan. 2022, Art. no. 131960, doi: 10.1016/j.chemosphere.2021.131960.

[5] S. G. Rhee, T.-S. Chang, W. Jeong, and D. Kang, "Methods for detection and measurement of hydrogen peroxide inside and outside of cells," *Molecules Cells*, vol. 29, no. 6, pp. 539–549, Jun. 2010, doi: 10.1007/s10059-010-0082-3.

[6] S. Jo, D. Sung, S. Kim, and J. Koo, "A review of wearable biosensors for sweat analysis," *Biomed. Eng. Lett.*, vol. 11, no. 2, pp. 117–129, May 2021, doi: 10.1007/s13534-021-00191-y.

[7] M. Majdinasab, M. Daneshi, and J. Louis Marty, "Recent developments in non-enzymatic (bio)sensors for detection of pesticide residues: Focusing on antibody, aptamer and molecularly imprinted polymer," *Talanta*, vol. 232, Sep. 2021, Art. no. 122397, doi: 10.1016/j.talanta.2021.122397.

[8] H. Karimi-Maleh, F. Karimi, M. Alizadeh, and A. L. Sanati, "Electrochemical sensors, a bright future in the fabrication of portable kits in analytical systems," *Chem. Rec.*, vol. 20, no. 7, pp. 682–692, Jul. 2020, doi: 10.1002/tcr.201900092.

[9] R. M. Trujillo, D. E. Barraza, M. L. Zamora, A. Cattani-Scholz, and R. E. Madrid, "Nanostructures in hydrogen peroxide sensing," *Sensors*, vol. 21, no. 6, p. 2204, 2021, doi: 10.3390/s21062204.

[10] E. Sardini, M. Serpelloni, and S. Tonello, "Printed electrochemical biosensors: Opportunities and metrological challenges," *Biosensors*, vol. 10, no. 11, p. 166, Nov. 2020, doi: 10.3390/bios10110166.

[11] Y. Zhou, C.-W. Chiu, and H. Liang, "Interfacial structures and properties of organic materials for biosensors: An overview," *Sensors*, vol. 12, no. 11, pp. 15036–15062, Nov. 2012, doi: 10.3390/s121115036.

[12] W. He, X. Ye, and T. Cui, "Flexible electrochemical sensor with graphene and gold nanoparticles to detect dopamine and uric acid," *IEEE Sensors J.*, vol. 21, no. 23, pp. 26556–26565, Dec. 2021, doi: 10.1109/JSEN.2021.3122326.

[13] K. K. Yeung, T. Huang, Y. Hua, K. Zhang, M. M. F. Yuen, and Z. Gao, "Recent advances in electrochemical sensors for wearable sweat monitoring: A review," *IEEE Sensors J.*, vol. 21, no. 13, pp. 14522–14539, Jul. 2021, doi: 10.1109/JSEN.2021.3074311.

[14] M. F. Md Shakhih, A. S. Rosslan, A. M. Noor, S. Ramanathan, A. M. Lazim, and A. A. Wahab, "Review-enzymatic and non-enzymatic electrochemical sensor for lactate detection in human biofluids," *J. Electrochem. Soc.*, vol. 168, no. 6, Jun. 2021, Art. no. 067502, doi: 10.1149/1945-7111/ac0360.

[15] T. Fapanni, E. Sardini, M. Serpelloni, and S. Tonello, "3D electrochemical sensor and microstructuration using aerosol jet printing," *Sensors*, vol. 21, no. 23, p. 7820, Nov. 2021, doi: 10.3390/s21237820.

[16] F. Mortazavi, N. Arab, and L. Fotouhi, "Signal amplification based on a polymeric film decorated with nanocomposites for sensitive determination of propranolol in biological and pharmaceutical samples," *IEEE Sensors J.*, vol. 21, no. 18, pp. 20850–20856, Sep. 2021, doi: 10.1109/JSEN.2021.3097384.

[17] I.-H. Cho, D. H. Kim, and S. Park, "Electrochemical biosensors: Perspective on functional nanomaterials for on-site analysis," *Biomater. Res.*, vol. 24, no. 1, pp. 1–12, Dec. 2020, doi: 10.1186/s40824-019-0181-y.

[18] C. Chen et al., "Development of micropillar array electrodes for highly sensitive detection of biomarkers," *RSC Adv.*, vol. 10, no. 67, pp. 41110–41119, 2020, doi: 10.1039/d0ra07694e.

[19] Q. Cao, P. Puthongkham, and B. J. Venton, "Review: New insights into optimizing chemical and 3D surface structures of carbon electrodes for neurotransmitter detection," *Anal. Methods*, vol. 11, no. 3, pp. 247–261, Jan. 2019, doi: 10.1039/c8ay02472c.

[20] X. Li, M. Xu, Q. Wu, W. Wei, and X. Liu, "Photolithographic 3D microarray electrode-based high-performance non-enzymatic H_2O_2 sensor," *Colloids Surf. A, Physicochem. Eng. Aspects*, vol. 628, Nov. 2021, Art. no. 127249, doi: 10.1016/j.colsurfa.2021.127249.

[21] X. Liu, Y. Zhou, J. Liu, and H. Xia, "The intrinsic enzyme mimetic activity of platinum oxide for biosensing of glucose," *Spectrochim. Acta A, Mol. Biomol. Spectrosc.*, vol. 248, Mar. 2021, Art. no. 119280, doi: 10.1016/j.saa.2020.119280.

[22] Y. Hu, M. Hojamberdiev, and D. Geng, "Recent advances in enzyme-free electrochemical hydrogen peroxide sensors based on carbon hybrid nanocomposites," *J. Mater. Chem. C*, vol. 9, no. 22, pp. 6970–6990, Jun. 2021, doi: 10.1039/d1tc01053k.

[23] M. Eryigit, B. Kurt Urhan, H. O. Dogan, T. O. Ozer, and U. Demir, "ZnO nanosheets-decorated ERGO layers: An efficient electrochemical sensor for non-enzymatic uric acid detection," *IEEE Sensors J.*, vol. 22, no. 6, pp. 5555–5561, Mar. 2022, doi: 10.1109/JSEN.2022.3150088.

[24] Y.-S. Huang, K.-Y. Chen, Y.-T. Cheng, C.-K. Lee, and H.-E. Tsai, "An inkjet-printed flexible non-enzymatic lactate sensor for clinical blood plasma test," *IEEE Electron Device Lett.*, vol. 41, no. 4, pp. 597–600, Apr. 2020, doi: 10.1109/LED.2020.2973343.

[25] N. Aliakbarinodehi et al., "Electrochemical nanostructured biosensors: Carbon nanotubes versus conductive and semi-conductive nanoparticles," *Chem. Papers*, vol. 69, no. 1, pp. 134–142, 2015, doi: 10.1515/chempap-2015-0004.

[26] L. Fan et al., "Green synthesis of stable platinum nanoclusters with enhanced peroxidase-like activity for sensitive detection of glucose and glutathione," *Microchem. J.*, vol. 166, Jul. 2021, Art. no. 106202, doi: 10.1016/j.microc.2021.106202.

[27] Á. Torrinha, T. M. B. F. Oliveira, F. W. P. Ribeiro, A. N. Correia, P. Lima-Neto, and S. Morais, "Application of nanostructured carbon-based electrochemical (bio)sensors for screening of emerging pharmaceutical pollutants in waters and aquatic species: A review," *Nanomaterials*, vol. 10, no. 7, pp. 1–29, 2020, doi: 10.3390/nano10071268.

[28] D. C. Ferrier and K. C. Honeychurch, "Carbon nanotube (CNT)-based biosensors," *Biosensors*, vol. 11, no. 12, p. 486, Nov. 2021, doi: 10.3390/bios11120486.

[29] L.-Y. Ma and N. Soin, "Recent progress in printed physical sensing electronics for wearable health-monitoring devices: A review," *IEEE Sensors J.*, vol. 22, no. 5, pp. 3844–3859, Mar. 2022, doi: 10.1109/JSEN.2022.3142328.
[30] G. K. Lau and M. Shrestha, "Ink-jet printing of micro-electro-mechanical systems (MEMS)," *Micromachines*, vol. 8, no. 6, p. 194, 2017, doi: 10.3390/mi8060194.
[31] S. Agarwala, G. L. Goh, and W. Y. Yeong, "Optimizing aerosol jet printing process of silver ink for printed electronics," in *Proc. IOP Conf., Mater. Sci. Eng.*, 2017, vol. 191, no. 1, Art. no. 012027, doi: 10.1088/1757-899X/191/1/012027.
[32] M. Borghetti, E. Cantù, E. Sardini, and M. Serpelloni, "Future sensors for smart objects by printing technologies in industry 4.0 scenario," *Energies*, vol. 13, no. 22, p. 5916, Nov. 2020, doi: 10.3390/en13225916.
[33] A. M. Faria, E. B. M. I. Peixoto, C. B. Adamo, A. Flacker, E. Longo, and T. Mazon, "Controlling parameters and characteristics of electrochemical biosensors for enhanced detection of 8-hydroxy-2'-deoxyguanosine," *Sci. Rep.*, vol. 9, no. 1, pp. 1–10, 2019, doi: 10.1038/s41598-019-43680-y.
[34] M. Chen et al., "Parallel, multi-material electrohydrodynamic 3D nanoprinting," *Small*, vol. 16, no. 13, pp. 1–7, 2020, doi: 10.1002/smll.201906402.
[35] S. Tonello et al., "Electrochemical detection of different p53 conformations by using nanostructured surfaces," *Sci. Rep.*, vol. 9, no. 1, pp. 1–14, 2019, doi: 10.1038/s41598-019-53994-6.
[36] G. Cho, S. Azzouzi, G. Zucchi, and B. Lebental, "Electrical and electrochemical sensors based on carbon nanotubes for the monitoring of chemicals in water—A review," *Sensors*, vol. 22, no. 1, p. 218, 2022, doi: 10.3390/s22010218.
[37] A. J. Bard and L. R. Faulkner, *Electrochemical Methods: Fundamentals and Applications*, 2nd ed. Hoboken, NJ, USA: Wiley, 2001.
[38] S. S. Ghoreishizadeh, G. Nanda, S. Carrara, and G. De Micheli, "Empirical study of noise dependence in electrochemical sensors," in *Proc. 5th IEEE Int. Workshop Adv. Sensors Interfaces (IWASI)*, Jun. 2013, pp. 36–39, doi: 10.1109/IWASI.2013.6576080.
[39] J. Heikenfeld et al., "Accessing analytes in biofluids for peripheral biochemical monitoring," *Nature Biotechnol.*, vol. 37, no. 4, pp. 407–419, 2019, doi: 10.1038/s41587-019-0040-3.
[40] S. Mutyala and J. Mathiyarasu, "A reagentless non-enzymatic hydrogen peroxide sensor presented using electrochemically reduced graphene oxide modified glassy carbon electrode," *Mater. Sci. Eng., C*, vol. 69, pp. 398–406, Dec. 2016, doi: 10.1016/j.msec.2016.06.069.
[41] N. Elgrishi, K. J. Rountree, B. D. McCarthy, E. S. Rountree, T. T. Eisenhart, and J. L. Dempsey, "A practical beginner's guide to cyclic voltammetry," *J. Chem. Educ.*, vol. 95, no. 2, pp. 197–206, Feb. 2018, doi: 10.1021/acs.jchemed.7b00361.
[42] D. F. de Queiroz, T. R. L. de Dadamos, S. A. S. Machado, and M. A. U. Martines, "Electrochemical determination of norepinephrine by means of modified glassy carbon electrodes with carbon nanotubes and magnetic nanoparticles of cobalt ferrite," *Sensors*, vol. 18, no. 4, p. 1223, 2018, doi: 10.3390/s18041223.
[43] Y. Lei, B. D. Ossonon, J. Chen, J. Perreault, and A. C. Tavares, "Electrochemical characterization of graphene-type materials obtained by electrochemical exfoliation of graphite," *J. Electroanal. Chem.*, vol. 887, Apr. 2021, Art. no. 115084, doi: 10.1016/j.jelechem.2021.115084.
[44] A. Shrivastava and V. B. Gupta, "Methods for the determination of limit of detection and limit of quantitation of the analytical methods," *Chronicles Young Sci.*, vol. 2, no. 1, p. 21, 2011, doi: 10.4103/2229-5186.79345.
[45] Z. Miao, D. Zhang, and Q. Chen, "Non-enzymatic hydrogen peroxide sensors based on multi-wall carbon nanotube/Pt nanoparticle nanohybrids," *Materials*, vol. 7, no. 4, pp. 2945–2955, Apr. 2014, doi: 10.3390/ma7042945.
[46] J. Ping, Y. Wang, K. Fan, J. Wu, and Y. Ying, "Direct electrochemical reduction of graphene oxide on ionic liquid doped screen-printed electrode and its electrochemical biosensing application," *Biosensors Bioelectron.*, vol. 28, no. 1, pp. 204–209, Oct. 2011, doi: 10.1016/j.bios.2011.07.018.
[47] A. Hassibi, R. Navid, R. W. Dutton, and T. H. Lee, "Comprehensive study of noise processes in electrode electrolyte interfaces," *J. Appl. Phys.*, vol. 96, no. 2, pp. 1074–1082, Jul. 2004, doi: 10.1063/1.1755429.
[48] S. Woo, Y. R. Kim, T. D. Chung, Y. Piao, and H. Kim, "Synthesis of a graphene–carbon nanotube composite and its electrochemical sensing of hydrogen peroxide," *Electrochim. Acta*, vol. 59, pp. 509–514, Jan. 2012, doi: 10.1016/j.electacta.2011.11.012.

Tiziano Fapanni (Student Member, IEEE) received the M.Sc. (*cum laude*) degree in electronic engineering from the University of Brescia, Brescia, Italy, in 2019, and the Ph.D. degree in technology for health from the Department of Information Engineering, University of Brescia.

His research interests include the development of sensors and conditioning circuit for e-skin application to monitor physiological and biochemical signals.

Emilio Sardini (Member, IEEE) received the M.Sc. degree in electronics engineering from the Politecnico di Milano, Milan, Italy, in 1983.

He was a member of the Academic Senate, the Board of Directors, and the University of the Brescia, Brescia, Italy. He was the Deputy Dean of the Engineering Faculty, the Director of the Department of Information Engineering, and a Coordinator of the Technology for Health Ph.D. Program. He is currently a Full Professor with the Department of Information Engineering, University of Brescia. His research interests include electronic instrumentation, sensors and signal conditioning electronics, and the development of autonomous sensors for biomedical applications.

Mauro Serpelloni (Senior Member, IEEE) received the M.S. (*cum laude*) degree in industrial management engineering and the Ph.D. degree in electronic instrumentation from the University of Brescia, Brescia, Italy, in 2003 and 2007, respectively.

He is currently a Full Professor with the Department of Information Engineering, University of Brescia. His current research interests include biomechatronic systems, contactless transmission, and signal processing for microelectromechanical systems.

Sarah Tonello (Member, IEEE) received the dual M.S. (*cum laude*) degree in biomedical engineering from the University of Florida, Gainesville, FL, USA, and the Politecnico di Milano, Milan, Italy, in 2014, as part of the dual degree program Atlantis CRISP, and the Ph.D. degree in technology for health from the University of Brescia, Brescia, Italy, in 2017.

She is currently a Researcher with the Department of Information Engineering, University of Padua, Padua, Italy. Her research interests include printed sensors, electronic devices, and electrochemical sensors.